Preparation of Rh−Graphite and Rh−Clay Nanocomposites: Model Substances for Nanographite and Induced Magnetization in 4d Transition Metals

Jürgen Walter,* Shinya Wakita, Wararat Boonchuduang, and Shigeta Hara

Department of Materials Science and Processing, Osaka University, 2-1 Yamada-oka, Suita, Osaka 565-0871, Japan

Masatsugu Suzuki and Itsuko Sato Suzuki

Department of Physics, State University of New York at Binghamton, Binghamton, New York 13902-6016

Received: January 24, 2002; In Final Form: April 12, 2002

Rh nanoparticles in a graphite lattice have been prepared by reduction of a $RhCl_3$−graphite intercalation compound by hydrogen gas at high temperatures (**I**) or at room temperature by Li−diphenylide (**II**). In all cases, the reduction was complete. All four samples (natural graphite and HOPG) showed a full set of fcc Rh reflections by selected-area electron diffraction. This indicates a particle thickness from at least four layers. Only in the case of the samples reduced by (**II**) can additional very strong reflections can be observed. They seem to be due to the occurrence of 2D Rh structures with $(2 \times a_{graphite})$ and $(3 \times a_{graphite})$ superstructures. For a $(2 \times a_{graphite})$ Rh superstructure on graphite or expanded multilayers of fcc Rh, an induced magnetic moment was theoretically predicted. Bright-field electron microscopy shows particles in the size ranges 11−106 nm (**I**) and 1.5−37.5 nm (**II**). The magnetism of Rh−Gr is related to the detail of Rh nanoparticles and nanographites, depending on the condition of reduction. Short-range magnetic order is observed in Rh nanoparticles for the sample with uncommon spacings. However, Curie-like susceptibility is observed at low temperatures for all samples. This is due to nanographites with zigzag edges. As reference substances, Rh nanoparticles were generated in bentonite and on kaolin by polyol reduction of Rh−acetate hydrate. The size range in bentonite was 2.1−60 nm; the kaolin samples showed Rh particles from 5.3−52.5 nm. Electron diffraction patterns gave no evidence of an expanded lattice in those Rh particles.

1. Introduction

Magnetic properties of metals are commonly considered to be nonchangeable. This is not true, as the latest research has demonstrated. Theoretic physicists predicted that several 4d transition metals might show induced magnetism because of the high susceptibility and high density of states near the Fermi edge of those metals. In particular, palladium is one hot candidate for these studies. However, all these papers varied about the conditions under which palladium should show a magnetic moment. Bouarab et al.[1] predicted ferromagnetism in Pd for slabs with thicknesses between 2 and 5 monolayers (ML). Slabs with more than five MLs or only one ML should be paramagnetic, according to their calculations.[1] However, Moruzzi and Marcus[2] concluded that face-centered cubic (fcc) Pd and fcc Rh should be ferromagnetic by lattice expansion. Also, Fritsche et al.[3] came to the same conclusion. Zhu et al.[4] calculated the same, but only for Pd monolayers. A possible magnetic offset was also published for small Pd clusters, depending on their particle sizes. Lee[5] predicted that Pd_{19} clusters with fcc structure or Pd_{15} clusters with body-centered cubic (bcc) symmetry should be ferromagnetic according to his calculation. Reddy et al.[6] published a ferromagnetic offset for 13-atom clusters of Pd, Rh, and Ru.

A magnetic moment[9,10] has been observed in quasi 2D Pd nanoparticles encapsulated in graphite.[11] Ferromagnetic as well as antiferromagnetic samples could be prepared.[10] Besides, common fcc Pd reflections could be occasionally observed from particles with a $(2 \times a_{graphite})$ or a $(3 \times a_{graphite})$ superstructure.[12,13] At least the latter superstructure shows a significant lattice expansion with respect to common fcc Pd. Those samples are also active catalysts for C−C coupling reactions.[14]

Rhodium clusters (Rh_n, $n = 12-32$) showed magnetic ordering of the 4d electrons, indicating a ferromagnetic ordering.[15] The clusters were formed by laser vaporization of a Rh sample.[15] Magnetic moments have been detected by following the passage of the clusters through a gradient magnetic field;[15] for details of the technique, see ref 16. The clusters were superparamagnetic at 93 K, with magnetic moments of between 0.3 and 1.1 μ_B per atom.[15] The authors observed that Rh_{15}, Rh_{16}, and Rh_{19} have magnetic moments per atom that are significantly larger than those of adjacent clusters of comparable size.[15] It should be noted that Reddy at al.[6] predicted a ferromagnetic ordering in Rh for 13-atom clusters.

Krüger et al.[7] calculated the magnetism of hexagonal Ru and Rh monolayers that were epitaxially adsorbed on the graphite (001) surface. A small magnetic moment in those layers is possible if the metal atoms come close enough in contact to the adjacent graphene plane.[7] All other monolayers of 4d elements on (001) graphite surfaces with a $(2 \times a_{graphite})$ superstructure are nonmagnetic, in agreement with calculations performed by Chen et al.[8] These authors also found that because of the unexpectedly strong interfacial interaction between the

* Corresponding author. E-mail: Juerg_Walter@t-online.de. Tel. and Fax: +49/6106/284946.

10.1021/jp0255278 CCC: $22.00
Published on Web 07/31/2002

overlayer and the flat (001) carbon substrate, the magnetic moment is very sensitive to changes in the interlayer distances.[8]

Pfandzelter et al.[17] observed a magnetic moment on a Ru monolayer deposited on a (001) face of highly oriented pyrolytic graphite (HOPG). Auger electron spectroscopy showed that the covering of the graphite surface was lateral until the monolayer was formed. The magnetic properties of the film were studied by spin-polarized secondary electron spectroscopy.[17] For one monolayer consisting of Ru on C(001), below a surface Curie temperature of approximately 250 K, nonzero in-plane polarization is observed and found to saturate in an applied field of a few tenths of an oersted.[17] The magnetic order indicated spontaneous 2D ferromagnetism in this Ru film, and the degree of magnetism is quite low.

Theoretical papers show the possibility of an induced magnetic moment in Rh or Ru layers on graphite substrates. In our approach, we use metal chloride graphite intercalation compounds (GICs) as precursor materials. In a GIC, one guest layer is sandwiched by two adjacent graphene (IUPAC nomenclature of a single carbon layer with graphitic properties) sheets.[18] The periodic sequence of GICs has been known since the 1930s. The carbon−metal−carbon sandwich may lead to larger magnetic moments if only a carbon substrate is used.

The reduction of metal chloride GICs by Li−diphenylide or hydrogen was established by Volpin and co-workers.[19,20] Because these 4d transition metal nanoparticles in graphite were often produced, they have been studied mainly in regard to their catalytic properties. To the best of our knowledge, structural (with the exception of ref 20) and magnetic investigations were not carried out. Depending on the metal chloride used, atoms,[21] molecules,[21] monolayers,[20] bilayers,[22] or multilayered particles[19,11] can be formed. Commonly, the reaction cannot be guided; it is a kind of self-organization. Particles with and without charge-transfer interaction with the graphite lattice can be prepared.[12]

The aims of the present paper are to prepare Rh slabs with a ($2 \times a_{graphite}$) superstructure, describe the samples by TEM/SAED, and show the first principle magnetic study. Because the formation of nanoparticles in the interlayer space is due to self-organization, we use different reduction methods. Because a much more detailed investigation of the magnetic properties of all samples would greatly extend the length of this manuscript, it will be published in a second paper.

2. Experimental Section

2.1. Rh−Graphite System. Highly oriented pyrolytic graphite, grade ZYA from Advanced Ceramics Corporation, Lakewood, OH, orpurified natural graphite (samples: Rh−Gr(2), Rh−Gr(3), and Rh−Gr(4)) from Graphitwerke Kropfmühl, Germany with 30-ppm Fe, 5-ppm Co, and 5-ppm Ni, according to Graphitwerke Kropfmühl) has been used as the host material. The graphite was placed in an ampule, and $RhCl_3$ from Tanaka Kikinzoku, Tokyo, Japan, was added. After evacuation, chlorine gas was condensed in the ampule before it was sealed. The mixture was heated at 240 °C for 3 days. Success of the intercalation was confirmed by a Rigaku RINT 2000 X-ray powder diffractometer operating at the following conditions: 40 kV, 200 mA, Cu Kα radiation, stepsize 0.02°. Reduction was performed by two different methods:

(i) Reduction by hydrogen gas. The GIC was placed in a flow reactor where hydrogen gas was continuously flowing; reduction time was 2 days. Sample Rh−Gr(1) was reduced at 400 °C, and sample Rh−Gr(3), at 300 °C.

(ii) Rh−Gr(2) and Rh−Gr(4) were reduced at room temperature for 2 days in Li−diphenylide. For this, in a glovebox, Li was added to a mixture of dry tetrahydrofuran (THF) and naphthalene. The reaction was started by a short period of sonification. As the clear solution turned dark, sonification was stopped, and $RhCl_3$−GIC was added.

During the synthesis of GICs, one should always be aware of the following hazards: (i) Ampules can explode; therefore, protect your eyes. (ii) Work in a hood; otherwise, the staff is exposed to chlorine gas if an ampule explodes. (iii) Before you open a sealed ampule, cool it down with liquid nitrogen so that the inside pressure is reduced.

All samples were studied by a Hitachi H-800 transmission electron microscope (TEM) with an accelerating voltage of 200 kV ($\lambda = 2.5$ pm including a relativistic corrugation). Selected-area electron diffraction (SAED) patterns were analyzed with different camera lengths, which are mentioned in the figure captions. Graphite reflections have been used as internal standards and for refinement of the camera constants. The DC magnetic susceptibility of Rh−Gr samples was measured using a SQUID magnetometer (MPMS XL-5, Quantum Design) with an ultralow-field capability option.

2.2. Rh−Clay System. We used two different kinds of clay minerals. Kaolin is composed of a two-sheet layer structure with zero net charge in the layers. Therefore, no ions were found between the layers. Kaolin was obtained from Kanto Chemical Co., Inc. Tokyo, Japan, with maximum 0.1% Cl and maximum 0.1% Fe. The second clay was bentonite from Kanto Chemical Co., Inc. Tokyo, Japan. An extra-pure grade of sodium-rich bentonite was used. Bentonite is the rock name used for the ore itself. The ore consists of clay minerals of the subgroup smectite and several impurities such as gravel, shale, or limstone. After purification, it is chemically montmorillonite or hectorite (depending on the origin). However, often the name bentonite is still used after purification. Montmorillonite is a layered Mg/Al−silicate with sheet morphology, and hectorite is a Mg−silicate with lath or strip morphology. The sample used in our experiment is chemically a montmorillonite. The platelets show a negative net charge; therefore, cations can be found between the layers.

The clay (1.75 g) was suspended in water (20 mL) with rhodium acetate dimer hydrate ($[(CH_3COO)_2Rh]_2 \cdot 2H_2O$),[34,35] first grade from Wako Pure Chemicals, Osaka, Japan (1.25 g). The solution was sonicated in a Yamato 1510J-MT ultrasonic bath (70 W, 42 kHz) for 1 day. Afterward, the solution was filtered, and the recipient was added to 20 mL of ethylene glycol and stored for 6 h in an ultrasonic bath again. Then the suspension was filtered and washed with methanol and dried at 70 °C. The samples were investigated by XRD and TEM/SAED under the same conditions as those used for Rh−graphite samples.

3. Results and Discussion

3.1. Rh−Graphite System.

3.1.1. Structural Characterization. After intercalation of $RhCl_3$, all samples still showed large graphite (002) and (004) reflections in X-ray diffraction patterns (XRD). This indicates that large graphite areas were not intercalated. After reduction of the $RhCl_3$−GIC, the sample was investigated by TEM, and bright field images can be seen for all four samples (Figure 1a−d), with a corresponding SAED pattern (Figure 1e−h). The graphite lattice shows large graphite areas that are not occupied by particles. Even domains with particles are distinguishable as densely populated. Most of the filled domains are found near the prismatic edges; some of them also appear deeper inside the graphite lattice.

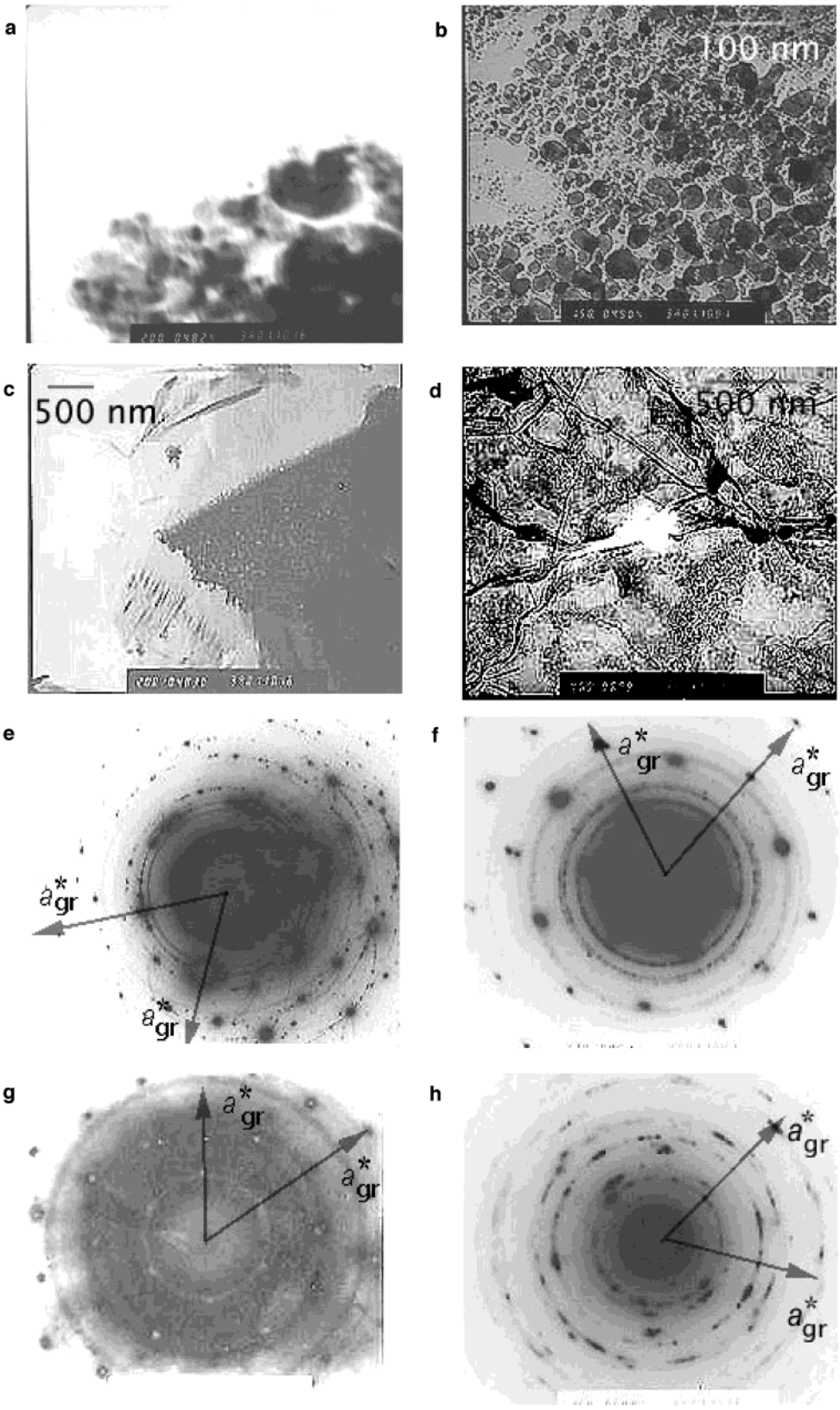

Figure 1. (a) Rh−Gr(1) reduced by hydrogen gas at 400 °C. Shown are some particles near the prismatic edges. (b) Rh−Gr(2) reduced by Li−diphenylide at room temperature. Shown is an area moderately densely populated by Rh nanoparticles. (c) Rh−Gr(3) reduced by hydrogen gas at 300 °C. A highly densely populated Rh domain (black) can be seen. (d) Rh−Gr(4) reduced by Li−diphenylide at room temperature. Shown are some Rh nanoparticles far away from the prismatic edges. (e) Corresponding SAED pattern in Figure 1a; for convenience, the axes of the graphite lattice are indicated; $\lambda = 2.5$ pm including a relativistic corrugation, and camera length = 0.8 m. (f) Corresponding SAED pattern in Figure 1b; for convenience, the axes of the graphite lattice are indicated; $\lambda = 2.5$ pm including a relativistic corrugation, and camera length = 1.2 m. (g) Corresponding SAED pattern in Figure 1c; for convenience, the axes of the graphite lattice are indicated; $\lambda = 2.5$ pm including a relativistic corrugation, and camera length = 1.2 m. (h) Corresponding SAED pattern in Figure 1d; for convenience, the axes of the graphite lattice are indicated; $\lambda = 2.5$ pm including a relativistic corrugation, and camera length = 1.6 m.

TABLE 1: Experimentally Observed Spacings after Hydrogen Reduction from Rh−Gr(1), Rh−Gr(3), and (*hkl*)[a]

$d_{Rh-Gr(1)}$/(pm)	$d_{Rh-Gr(3)}$/(pm)	(*hkl*)
not observed	219.8	111
188.7	186.5	200
166.7	not observed	?
130.2	132.3	220
117.6	112.9	311
108.1	108.0	222
92.4	91.2	400
83.3	84.3	331
79.2	82.1	420

[a] Graphite reflections were not considered but were used as as internal standard and for refinement of the camera constant. All Rh reflections can be indexed as common fcc (PDF: 5−685). The (111) reflection in Rh−Gr(1) cannot be observed because the camera constant (0.8 m) was too small. The unknown reflection (d = 166.7 pm) was not observed in Rh−Gr(3).

TABLE 2: Experimentally Observed Spacings after Li−Diphenylide Reduction from Rh−Gr(2), Rh−Gr(4), and (*hkl*)[a]

$d_{Rh-Gr(2)}$/(pm)	$d_{Rh-Gr(4)}$/(pm)	(*hkl*)
not observed	421.1	$(100)_{hex2a}$
313.2	296.3	$(200)_{hex3a}$
274.1	262.3	?
223.0	216.2	$(111)_{fcc}$
212.0	210.5	$(300)_{hex3a}$
190.7	179.8	$(200)_{fcc}$
162.4	not observed	?
154.8	153.8	$(400)_{hex3a}$
not observed	145.5	$(300)_{hex2a}$
131.6	127.0	$(220)_{fcc}$
120.7	115.9	$(311)_{fcc}$
103.8	103.5	$(600)_{hex3a}$
102.8	not observed	$(400)_{fcc}$
87.7	not observed	$(331)_{fcc}$

[a] Graphite reflections were not considered but were used as as internal standard and for refinement of the camera constant. One part of the diffraction rings is identical to fcc Rh (PDF: 5−685). Other reflections could be indexed if a ($2 \times a_{graphite}$) superstructure (hex2a) or a ($3 \times a_{graphite}$) superstructure (hex3a) are assumed; see text.

All SAED patterns (Figure 1e−h) consist of polycrystalline diffraction rings for the Rh lattice, where point reflections denote the graphite lattice. Carbon reflections are used as an internal standard. In all four samples, a full series of fcc Rh reflections could be observed, in accordance with powder diffraction file (PDF) 5-685. The reduction was complete, and no unreacted $RhCl_3$−GIC domains could be detected. All polycrystalline diffraction rings of the hydrogen-reduced samples can be explained by fcc Rh reflections (see Table 1); sample Rh−Gr-(1) shows only one reflection that cannot be indexed. Samples Rh−Gr(1) and Rh−Gr(3) consist of multilayered fcc Rh particles. Those particles are much thicker, as in the other two samples. No reflections for RhH (PDF 45-1029) have been observed. Samples Rh−Gr(2) and Rh−Gr(4) reduced by Li−diphenylide show all prominent fcc Rh reflections (Figure 1f and g). However, these diffraction rings are not the only ones, and they are not the strongest. The most pronounced diffraction rings in Figure 1f do not belong to fcc Rh. These rings show larger spacings, as to be expected (see Table 2).

The following phases can be ruled out for remaining reflections (Figure 1f and g): fcc Rh (PDF 5-685), $RhCl_3$ (PDF 22-1255), LiCl (PDF 4−664, formed by the reaction with Li-diphenylide), Rh_2O_3 (PDF 43-1025), β−Rh_2O_3 (PDF 43-9), and RhO_2 (PDF 43-1026). Metal particles in graphite with mono- or bilayer thickness often form hexagonal arrangements; such agglomerations show hexagonal SAED patterns,[21,12] which are distinguishable to common fcc reflections. In such cases, often a ($2 \times a_{graphite}$)[21] or a ($3 \times a_{graphite}$)[12] superstructure can be observed. Therefore, we attempted to index the remaining reflections in this way. Some spacings from Table 2 that have not been indexed yet could be indexed as hexagonal if a ($2 \times a_{graphite}$) superstructure is assumed; others can be indexed if a ($3 \times a_{graphite}$) superstructure is assumed. Only two weak reflections cannot be indexed by this attempt. They could belong to a ($4 \times a_{graphite}$) superstructure. In this case, the larger spacings could not be observed because of the camera constant. We observed graphite reflections and a series of fcc Rh reflections. However, in this SAED pattern, additional and very strong reflections appear. The experiment can be repeated with the same result. These reflections indicate the possible occurrence of hexagonal islands (mono- or bilayers of Rh). This was confirmed for other elements (e.g., Pd[12] or Se[21]). Samples with 2D structures were always prepared at room temperature. It is likely that the low temperature of preparation leads to those 2D agglomerations. The ($2 \times a_{graphite}$) superstructure could be the early stage of the nanoparticle formation. If a fcc crystal grows up on the basal plane of graphite, then the (111) plane shows almost a ($2 \times a_{graphite}$) superstructure. The occurrence of a ($3 \times a_{graphite}$) superstructure is due to a self-organization process. Why are the spacings in Table 1 slightly different although we compare fcc Rh reflections, and why are the spacings in Table 2 different although we compare there the same superstructures? Spacings in nanoparticles depend on their particle sizes.[23] Commonly, very small and 2D bodies show lattice contraction. In the literature, lattice contraction up to 12%[24,25] in regard to bulk materials has been reported.[26,27] This effect was known long before nanotechnology became a hot topic.[28,29] Therefore, even in one graphite flake, the measured Rh spacings differ, and they are correlated to the Rh particle size. The same behavior was also observed by Pd nanoparticles encapsulated in graphite.[13]

Multilayered Rh nanoparticles with at least four MLs in thickness should generate internal stress inside the graphite lattice. The lateral dimension ranges from 11.0−106 nm (average particle size: 30.6 nm ± 20.7 nm, 41 particles considered) for hydrogen-prepared samples and from 1.5−37.5 nm (average particle size: 6.02 nm ± 4.5 nm, 310 particles considered) for Li−diphenyide-prepared samples. The particles must be at least four layers thick because the fcc unit cell can be only build up by three layers; for fcc reflections, at least one additional layer is required. Internal stress was observed in mono- or bilayer-thick Pd slabs in graphite by Raman spectroscopy.[12] Therefore, the Rh particles are thicker. It can be assumed that the internal stress inside the carbon lattice is more pronounced. What is the advantage of this? Graphite is diamagnetic, but so-called nanographite should show unique electronic and magnetic properties[30−32] depending on the edge state (armchair or zigzag type) of the nanosized graphene sheets. According to theoretical predictions, zigzag edges should exhibit a special edge state with a sharp peak in the density of states (DOS) at the Fermi energy. Pauli paramagnetism is predicted for nanographites showing Curie-like behavior at low temperatures.[31] Very recently, ferromagnetic rhombohedral C_{60} samples[33] have been described.[33] The multilayered Rh nanoparticles could generate enough internal stress in the graphite lattice that adjacent graphene sheets break and nanographites are formed. Therefore, Rh−graphite samples can be also used as model substances for so-called nanographites.

3.1.2. Magnetic Properties. In Rh−Gr, Rh nanoparticles are sandwiched between adjacent sheets of nanographites. Both nanographites and Rh nanoparticles contribute to the magnetism of Rh−Gr. A pristine Rh metal has a large paramagnetic susceptibility with an enhanced Stoner factor.[2] Theoretically, it is predicted that the 4d metals (Pd, Rh, Ru) may undergo a change of state from paramagnetic to ferromagnetic when the systems are formed of layers or finite clusters.[1,6,7] Nanographites are nanometer-sized graphite fragments representing a new class of mesoscopic systems that is intermediate between aromatic molecules and extended graphite sheets. Fujita and coworkers[30−32] have predicted that the electronic structures of finite-size graphene sheets depend crucially on the shape of their edges. The graphene edge of an arbitrary shape consists of two types of edges, zigzag and armchair, where the former has a *trans*-polyacetylene-type structure and the latter has a *cis*-polyacetylene-type structure. Finite graphite systems having zigzag edges exhibit a special edge state. The corresponding energy bands are almost flat at the Fermi energy E_F, thereby giving a sharp peak in the density of states (DOS) at E_F. This is in contrast to the case of a 2D graphene sheet with an infinite size, in which DOS is zero at E_F. In nanographites, the conduction electrons are localized near the zigzag edges, forming localized magnetic moments. These magnetic moments give rise to a Curie-like susceptibility only at low temperatures.[32]

In the present work, the magnetic susceptibility measurements of Rh−Gr were carried out as a part of sample characterization. The magnetism of Rh−Gr is expected to be related to the detail of Rh nanoparticles and nanographites, depending on the condition of reduction. The results are briefly discussed in terms of the above model. Figure 2a shows the DC magnetic susceptibility of Rh−Gr(1) at an external magnetic field $H =$ 50 Oe. After the sample was cooled from 298 to 1.9 K at $H =$ 0, $H = 50$ Oe was applied at 1.9 K. A zero-field-cooled (ZFC) magnetic susceptibility χ_{ZFC} was measured with increasing T from 1.9 to 50 K. The noisy signal is partly due to the small amount of sample used in this measurement. The susceptibility χ_{ZFC} shows a broad peak around 5.5 K, suggesting possible short-range ferromagnetic order in Rh nanoparticles. The susceptibility χ_{ZFC} is equal to -6×10^{-5} emu/g at 50 K and is almost independent of T at higher temperatures. This value of FC is comparable to the susceptibility of the pristine graphite along the c axis (-2.93×10^{-5} emu/g at 30 K), which is dominated by the orbital diamagnetic susceptibility due to the orbital motion of conduction electrons.

Figure 2b shows the T dependence of χ_{ZFC} and the field-cooled (FC) susceptibility χ_{FC} of Rh−Gr(2). The susceptibility χ_{ZFC} was measured with increasing T from 1.9 to 298 K. Subsequently, χ_{FC} was measured with decreasing T from 298 to 1.9 K. Both susceptibilities, which are diamagnetic at any T, exhibit a local minimum around 20 K. The susceptibility χ_{ZFC} deviates from χ_{FC} below 298 K, reflecting the frustrated nature of this system. Figure 2c shows the susceptibility of Rh−Gr(2) at $H = 10$ Oe. The susceptibility χ_{ZFC} shows a broad peak around 9.7 K at $H = 10$ Oe. This peak becomes a shoulder for H larger than 30 Oe. These results suggest short-range ferromagnetic order in Rh nanoparticles. The T dependence of χ_{FC} at $H = 10$ kOe obeys the Curie−Weiss law,

$$\chi_{FC} = \chi_0 + \frac{C}{T - \theta} \qquad (1)$$

in a limited T range ($5 \le T/\mathrm{K} \le 30$). The least-squares fit of the data of χ_{FC} versus T to eq 1 yields the Curie−Weiss temperature $\theta = -2.72 \pm 0.05$ K, the Curie−Weiss constant $C = (6.69 \pm 0.05) \times 10^{-6}$ emuK/g, and the T-independent susceptibility $\chi_0 = (-6.889 \pm 0.002) \times 10^{-6}$ emuK/g. Such Curie-like susceptibility at low temperatures may be due to the localized magnetic moments of conduction electrons near zigzag edges of nanographites.[32] The small value of $|\chi_0|$ is also consistent with the prediction[32] that the orbital motion of conduction electrons is suppressed in nanographites with zigzag edges.

Figure 2d shows the T dependence of χ_{ZFC} and χ_{FC} at $H =$ 10 Oe for Rh−G(3). The susceptibility χ_{ZFC} was measured with increasing T from 1.9 to 50 K. The sample was annealed at 70 K. Subsequently, χ_{FC} was measured with decreasing T from 50 to 1.9 K. No peak is observed in χ_{ZFC} at any T. The least-squares fit of the data of χ_{FC} versus T at $H = 1$ kOe to eq 1 yields $\theta =$ 0.46 ± 0.33 K, $C = (4.30 \pm 0.32) \times 10^{-6}$ emuK/g, and $\chi_0 =$ $(-6.453 \pm 0.015) \times 10^{-6}$ emuK/g. These values of θ, C, and χ_0 are comparable to those for Rh−Gr(2).

Figure 2e shows the T dependence of χ_{ZFC} and χ_{FC} at $H =$ 30 Oe for Rh−Gr(4). The susceptibility χ_{ZFC} was measured with increasing T from 1.9 to 298 K, and χ_{FC} was measured with decreasing T from 298 to 1.9 K. The sign of χ_{FC} changes from negative to positive at 6.4 K with decreasing T. No peak is observed at any T for either χ_{ZFC} or χ_{FC}. The susceptibility χ_{FC} at $H = 1$ kOe obeys the Curie−Weiss law at low temperatures. The least-squares fit of the data to eq 1 for ($5 \le T/\mathrm{K} \le 20$) yields $\theta = -0.76 \pm 0.07$ K, $C = (5.35 \pm 0.07) \times 10^{-6}$ emuK/g, and $\chi_0 = (-9.529 \pm 0.027) \times 10^{-7}$ emu/g. These values of C and θ are on the same order as those for Rh−Gr(2) and Rh−Gr(3). The smallest value of $|\chi_0|$ in Rh−Gr(4) indicates the strong suppression of the orbital motion of conduction electrons near zigzag edges of nanographites.

Figure 2f shows the hysteresis loop of the magnetization $M(H)$ at $T = 1.9$ K for Rh−Gr(2). After the sample was cooled from 298 to 1.9 K at $H = 0$, the magnetization $M(H)$ was measured ($-1 \le H/\mathrm{kOe} \le 1$). The magnetization curve at 1.9 K is dominated by the diamagnetic contribution, $\chi_d H$, with $\chi_d =$ -3.575×10^{-6} emu/g. Figure 2g shows the hysteresis loop of M defined by $\Delta M = M(H) - \chi_d \, \mathrm{d}H$. Although the loop of ΔM versus H is rather different from that of ideal ferromagnets, it still exhibits ferromagnetic character. This result also supports the fact that Rh nanoparticles are ferromagnetically ordered in Rh−Gr(2). It should be mentioned that all samples were prepared from materials out of the same batch. Therefore, if impurities exist, they are the same for all samples. However, only the sample with uncommonly large spacings for Rh shows a magnetic anomaly. This demonstrates that the observed effect is not due to impurities; it is likely due to the occurrence of Rh nanoparticles with uncommonly large spacings. A much more detailed magnetic characterization of all samples (including the Rh−clays) will be published elsewhere.

In summary, the Curie-like susceptibility is observed at low temperatures in all Rh−Gr samples. Their characteristic behavior is strongly dependent on the nature of the nanographites. A bit of evidence for short-range magnetic order in Rh nanoparticles is observed in χ_{ZFC} of Rh−Gr(2). The origin of such order may be related to the structure that has uncommnon spacings. Further experimental and theoretical studies are required to determine the relationship between the structure and magnetic order of Rh nanoparticles.

3.2. Rh−Clay Samples. The Rh−bentonite sample shows up in bright-field images of the nanoparticle (Figure 3a), and the corresponding SAED image shows diffraction rings for bentonite and fcc Rh. The Rh reflections are a little weak, but at least the Hanawalt group of Rh (PDF no. 5-0685) was

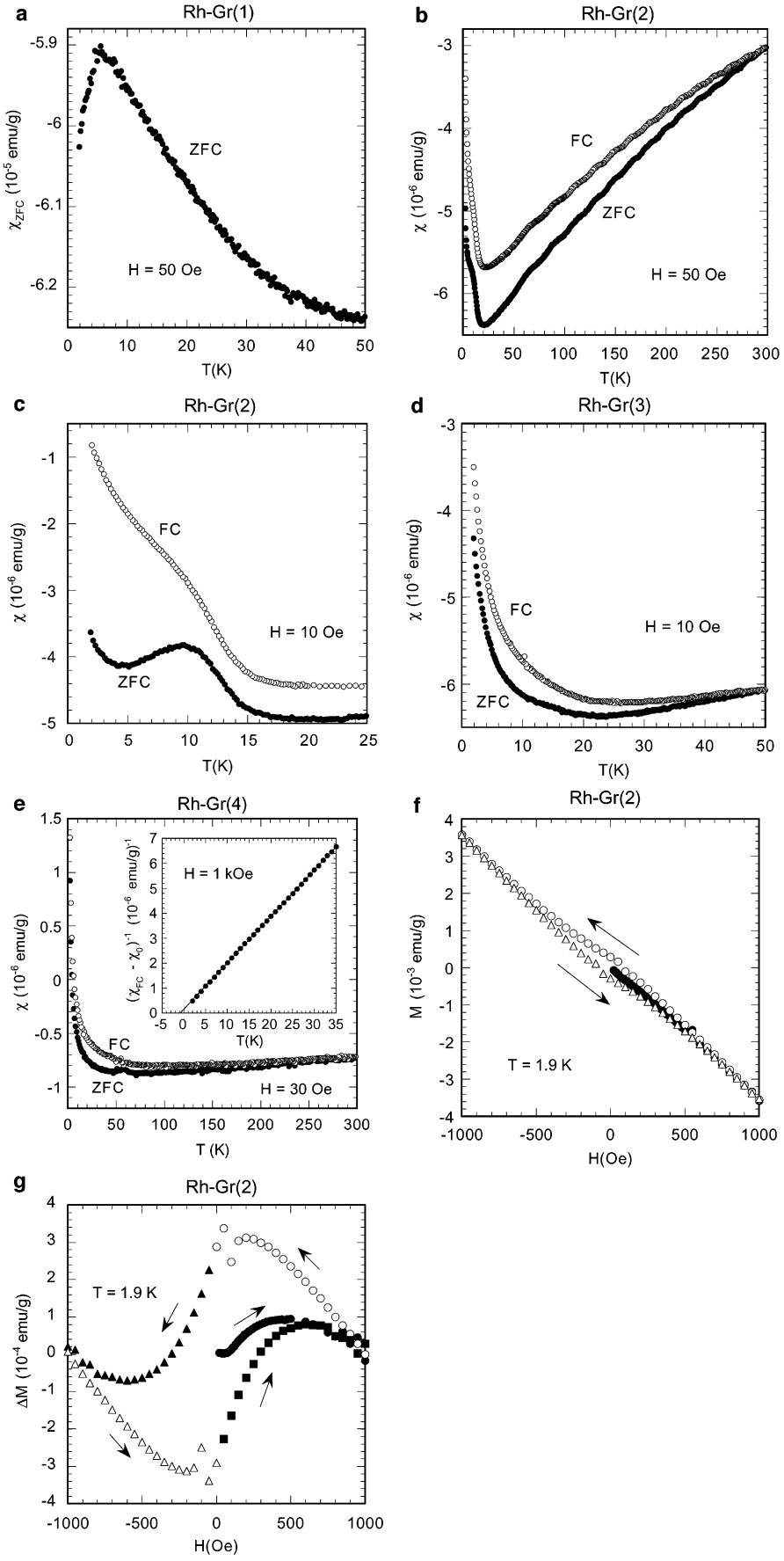

Figure 2. (a) T dependence of χ_{ZFC} for Rh−Gr(1) at $H = 50$ Oe. (b) T dependence of χ_{ZFC} and χ_{FC} at $H = 50$ Oe for Rh−Gr(2). (c) T dependence of χ_{ZFC} and χ_{FC} at $H = 10$ Oe for Rh−Gr(2). (d) T dependence of χ_{ZFC} and χ_{FC} at $H = 10$ Oe for Rh−Gr(3). (e) T dependence of χ_{ZFC} and χ_{FC} at $H = 30$ Oe for Rh−Gr(4). The inset shows the T dependence of $(\chi_{FC} - \chi_0)^{-1}$ at $H = 1$ kOe, where $\chi_0 = -9.529 \times 10^{-7}$ emu/g. (f) M vs H at 1.9 K for Rh−Gr(2) (-1 kOe $\leq H/\text{kOe} \leq 1$). (g) ΔM vs H at 1.9 K for Rh−Gr(2). $\Delta M = M - \chi_d H$ with $\chi_d = -3.575 \times 10^{-6}$ emu/g.

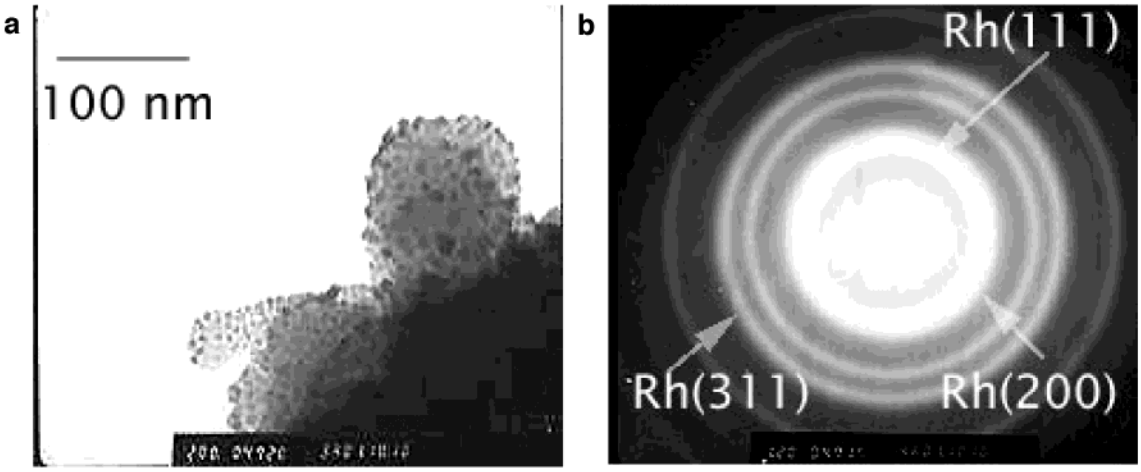

Figure 3. (a) Bright-field image of Rh−bentonite. (b) Corresponding SAED pattern; $\lambda = 2.5$ pm including a relativistic corrugation, and camera length = 1.2 m. The Hanawalt group is indicated.

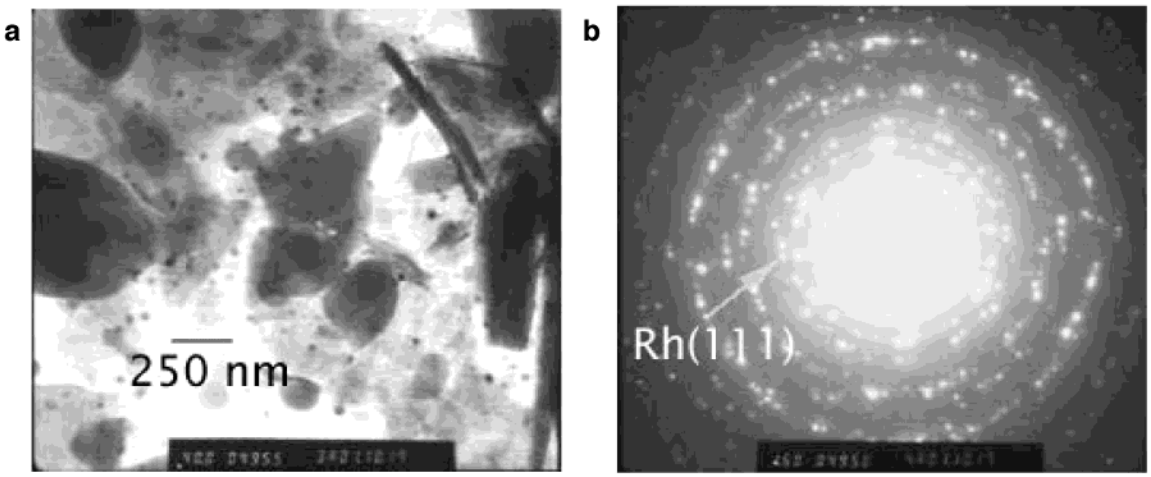

Figure 4. (a) Bright-field image of Rh−kaolin. Only the tiny particles consist of Rh. (b) Corresponding SAED pattern; $\lambda = 2.5$ pm including a relativistic corrugation, and camera length = 1.6 m. The occupation of the area is very low; therefore, only the Rh(111) reflection (100%) peak can be observed.

observed (Figure 3b). Rh−kaolin can be seen in Figure 4a, the corresponding SAED pattern, in Figure 4b. Also, this diffraction pattern shows polycrystaline rings for the clay and Rh. Unfortunately, only the Rh (111) reflection can be observed. No additional spacing exists. All other Rh reflections are too weak.

Every Rh reflection from Rh−clay samples showed the same spacings as those reported in PDF 5-0685. Therefore, the minimum thickness of those particles is also four layers. The lateral size was, in case of the bentonite sample, in the range from 2.1 to 60 nm (average particle size: 13.2 nm ± 10.0 nm, 148 particles considered), and the kaolin sample showed particles from 5.3 to 52.5 nm (average particle size: 22.0 nm ± 11.1 nm, 161 particles considered). No evidence of an expanded Rh lattice was found.

What is the advantage of Rh−clay? In the case of Rh−graphite composites, an unexpected strong interaction between a flat graphite basal plane and Rh is predicted,[7,8] which should lead to induced magnetism in the 4d metal. Even if no theoretic work exists for Rh−clay composites, we believe, in view of the work on graphite, that it is worthwhile to prepare Rh−clays. These samples have not yet been studied by SQUID. However, we will publish a much more detailed magnetic study on those systems soon.

4. Conclusions

Theoreticians have calculated the magnetic moment in a Rh ML on a graphite substrate with a $(2 \times a_{graphite})$ superstructure.[7,8] Multilayer systems on graphite have not been calculated until now. Experimentally, we observed in hydrogen-reduced samples only fcc Rh nanoparticles. Those particles consist of multilayers, and these samples show no magnetic ordering. Some particles in Li−diphenylide-reduced samples show additional reflections that could be indexed as 2D structures with a $(2 \times a_{graphite})$ or a $(3 \times a_{graphite})$ superstructure. If a fcc Rh lattice is grown up with the (111) face, the superstructure of the first ML is nearly a $(2 \times a_{graphite})$ superstructure. The zero-field susceptibility of Rh−Gr(2) shows a broad peak around 9.7 K, suggesting short-range magnetic order in Rh atoms. The fact that only samples with enlarged spacings showed this behavior indicates that the observed effect is not attributed to impurities but rather to structural changes in the particles. A much more detailed magnetic study will be reported elsewhere. The occurrence of magnetic ordering in Rh nanoparticles in samples with enlarged spacings in regard to common fcc Rh is in good agreement with theoretical predictions.[2,3,7,8] Therefore, the Rh−graphite samples can be considered to be model substances in the investigation of induced magnetic moments in Rh.

However, we know that particles in Rh−Gr(1) and Rh−Gr-(3) were at least four MLs in thickness. This must generate internal stress to the adjacent graphene sheets. Pronounced stress in graphene sheets adjacent to mono- and bilayers of Pd could be observed.[12] It is likely that adjacent graphene sheets will break off and nanographite will be formed. Theoretic papers[30−32] predicted unique electronic states and magnetic properties in nanographite. The observed Curie-like susceptibility at low temperatures may be due to the edge states of nanographites existing in Rh−graphite. Therefore, the Rh−graphites can also be considered to be model substances for this material.

Acknowledgment. J.W., S.W, W.B., and S.H. acknowledge financial support from the Ministry of Cultural Affairs, Education and Sport, Tokyo, Japan, under the grant for young scientists no. 70314375 and from Kansai Invention Center, Kyoto, Japan. The work at Binghamton was supported by the Research Foundation of SUNY−Binghamton (contract no. 240-9522A). We are grateful to Advanced Ceramics Corp. Lakewood, OH, Graphitwerke Kropfmühl, Germany, and Tanaka Kikinzoku, Tokyo, Japan, for providing us with materials.

References and Notes

(1) Bouarab, S.; Demangeat, C.; Mokrani, A.; Dreyssé, H. *Phys. Lett. A* **1990**, *151*, 103.
(2) Moruzzi, V. L.; Marcus, P. M. *Phys. Rev. B* **1989**, *39*, 471.
(3) Fritsche, L.; Noffke, J.; Eckardt, H. *J. Phys. F: Met. Phys.* **1987**, *17*, 943.
(4) Zhu, J.; Bylander, D. M.; Kleinman, L. *Phys. Rev. B* **1990**, *42*, 2874.
(5) Lee, K. *Phys. Rev. B* **1998**, *58*, 2391.
(6) Reddy, B. V.; Khanna, S. N.; Dunlap, B. I. *Phys. Rev. Lett.* **1993**, *70*, 3323.
(7) Krüger, P.; Parlebas, J. C.; Moraitis, G.; Demangeat, C. *Comput. Mater. Sci.* **1998**, *10*, 265.
(8) Chen, L.; Wu, R.; Kioussis, N.; Blanco, J. R. *J. Appl. Phys.* **1997**, *81*, 4161.
(9) Mendoza, D.; Morales, F.; Escudero, E.; Walter, J. *J. Phys.: Condens. Matter* **1999**, *11*, L317.
(10) Suzuki, M.; Suzuki, I. S.; Walter, J. *Phys. Rev. B* **2000**, *62*, 14171.
(11) Walter, J.; Shioyama, H. *Phys. Lett. A* **1999**, *254*, 65.
(12) Walter, J. *Philos. Mag. Lett.* **2000**, *80*, 257.
(13) Walter, J. *Adv. Mater.* **2000**, *12*, 31.
(14) Walter, J.; Heiermann, J.; Dyker, G.; Hara, S.; Shioyama, H. *J. Catal.* **2000**, *189*, 449.
(15) Cox, A. J.; Louderback, J. G.; Bloomfield, L. A. *Phys. Rev. Lett.* **1993**, *71*, 923.
(16) Bucher, J. P.; Douglass, D. C.; Xia, P.; Haynes, B.; Bloomfield, L. A. *Z. Phys. D: At., Mol. Clusters* **1991**, *19*, 251.
(17) Pfandzelter, R.; Steierl, G.; Rau, C. *Phys. Rev. Lett.* **1995**, *74*, 3467.
(18) Walter, J.; Shioyama, H. *J. Phys.: Condens. Matter* **1999**, *11*, L21.
(19) Vol'pin, M. E.; Novikov, Yu. N.; Lapkina, N. D.; Kasatochkin, V. I.; Struchkov, Yu. T.; Kasakov, M. E.; Stukan, R. A.; Povitskij, V. A.; Karimov, Yu. S.; Zvarikina, A. V. *J. Am. Chem. Soc.* **1975**, *97*, 3366.
(20) Shuvayev, A. T.; Helmer, Yu. B.; Lyubeznova, T. A.; Kraizman, V. L.; Mirmilstein, A. S.; Kvacheva, L. D.; Novikov, Yu. N.; Vol'pin, M. E. *J. Phys. (Orsay, Fr)* **1989**, *50*, 1145.
(21) Walter, J.; Shioyama, H. *J. Phys.: Condens. Matter* **2000**, *12*, 367.
(22) Walter, J.; Nishioka, M.; Hara, S. *Chem. Mater.* **2001**, *13*, 1828.
(23) Finch, G. I.; Fordham, S. *Proc. Phys. Soc., London* **1936**, *48*, 85.
(24) Sun, C. Q. *J. Phys.: Condens. Matter* **1999**, *11*, 4801.
(25) Yu, X. F.; Liu, X.; Zhang, K.; Hu, Z. Q. *J. Phys.: Condens. Matter* **1999**, *11*, 937.
(26) Højrup Hansen, K.; Worren, T.; Stempel, S.; Lægsgaard, E.; Bäumer, M.; Freund, H. J.; Besenbacher, F.; Stensgaard, I. *Phys. Rev. Lett.* **1999**, *83*, 4120.
(27) Klimenkov, M.; Nepijko, S.; Kulenbeck, H.; Bäumer, M.; Schlögl, R.; Freund, H. J. *Surf. Sci.* **1997**, *391*, 27.
(28) Goldschmidt, V. M. *Ber. Dtsch. Chem. Ges.* **1927**, *60*, 1270.
(29) Pauling, L. *J. Am. Chem. Soc.* **1947**, *69*, 542.
(30) Fujita, M.; Wakabayashi, K.; Nakada, K.; Kusakabe, K. *J. Phys. Soc. Jpn.* **1996**, *65*, 1920.
(31) Wakabayashi, K.; Fujita, M.; Ajiki, H.; Sigrist, M. *Phys. Rev. B* **1999**, *59*, 8271.
(32) Wkabayashi, K.; Sigrist, M.; Fujita, M. *J. Phys. Soc. Jpn.* **1998**, *67*, 2089.
(33) Markarova, T. L.; Sundquist, B.; Höhne, R.; Esquinazi, P.; Kopelevich, Y.; Scharff, P.; Davydov, V. A.; Kashevarova, L. S., Rakhmanina, A. V. *Nature (London)* **2001**, *413*, 716.
(34) Ayyappan, S.; Subbanna, G. N.; Srinivasa Gopalan, R.; Rao, C. N. R. *Solid State Ionics* **1996**, *84*, 271.
(35) Drljaca, A.; Spiccia, L.; Anderson, J. R.; Turney, T. W. *Inorg. Chim. Acta* **1997**, *254*, 219.